



Rainwater rivulets running on a stay cable subject to wind

Cécile Lemaitre*, Emmanuel de Langre, Pascal Hémon

Department of Mechanics, LadHyX, CNRS–Ecole Polytechnique, 91128 Palaiseau, France

ARTICLE INFO

Article history:

Received 30 July 2008

Received in revised form

24 February 2010

Accepted 26 February 2010

Available online 21 March 2010

Keywords:

Rivulet

Cable

Wind

Rain–wind-induced vibrations

ABSTRACT

Stay cables are likely to vibrate under the combined effect of rain and wind in the so-called phenomenon rain–wind-induced vibrations (RWIVs). Rain takes part in the phenomenon in the shape of water rivulets that run along the cables. In previous articles, the authors investigated the conditions under which such rivulets can be formed. Using a lubrication model, it was shown for a particular wind–cable configuration that rivulets can only be exhibited above a critical wind speed for which gravity is overcome. The rivulets' position was also predicted with the model. The results were validated by experiments.

In this paper, the wind speed at which rivulets appear and their position are expressed for an arbitrary wind–cable orientation. A maximum wind speed for the rivulets' existence is then estimated as the result of a balance between the drag force and the surface tension. A wind speed interval is consequently obtained for the rivulets' appearance and maintenance on a cylinder. The boundaries of this interval are expressed in term of Weber numbers, comparing the surface tension and wind effect. These predictions are successfully compared with all the measurements that have been published in the literature.

© 2010 Elsevier Masson SAS. All rights reserved.

1. Introduction

1.1. Rain–wind-induced vibrations

The cables of cable-stayed bridges are known to vibrate under the effect of wind. This is explained by several distinct mechanisms that are described by the theory of aeroelasticity, [1–5]. It was however discovered in the late 1970s [6] that cables are likely to vibrate due to a combination of rain and wind. Some authors have reported that vibrations stop [7] or are severely diminished [8,9] when rain disappears, showing the crucial role of rain water flow. This phenomenon was thus named rain–wind-induced vibrations (RWIVs). Bridge designers are eager to provide counter-measures against these vibrations in order to decrease the fatigue in cable systems and to reduce maintenance costs.

Observations show that the vibrations only occur for cables with an inclination towards the direction of the wind [7]. The stay cables generally vibrate transversely to the wind direction. Only low vibration modes are excited and the vibration frequencies range between 1 and 7 Hz [7].

The wind speed U necessary to initiate the phenomenon falls between 5 and 17 m/s. Unlike den Hartog galloping [10], which is due solely to wind and is not limited in wind speed, RWIVs are a velocity-restricted phenomenon. As a consequence, the RWIV

Reynolds number $Re = 2UR/\nu_a$ ranges between 7×10^4 and 2×10^5 for a usual cable radius of $R = 0.1$ m, $\nu_a = 1.5 \times 10^{-5}$ m²/s being the air kinematic viscosity.

Outdoors observations have been performed [7,11] that demonstrated the existence of one or two rivulets running along cables undergoing RWIVs (Fig. 1). RWIVs have been reproduced in wind tunnels with artificial rain, [7,12–16], which confirmed the necessity to have at least one rivulet for the excitation to occur. It was further observed that, in the absence of wind, a rivulet forms under a wet cable due to gravity; when the wind blows, this gravity rivulet shifts leeward and a second rivulet appears at the top of the cable [7]; see Fig. 1. By locally pouring some liquid on a cable only subjected to wind, it has been highlighted that the upper rivulet alone is sufficient for RWIVs [7].

Rivulets have been observed on full-scale cables in wind tunnels [17,18]. They are composed of a liquid carpet on which a hump evolves during the cable vibration (Fig. 1). The dimensions of a rivulet depend on the intensity of the rain, i.e. on the water flux supplied to the rivulet. The width of the wet base is typically centimetric, $0.8 < L < 3.8$ cm and the height of the hump is of the order of one millimetre, $0.5 < h < 2$ mm.

1.2. Models

Several models have been proposed to account for RWIVs. Most of them rely on the quasi-steady assumption that the cable displacement takes place at much lower speeds than the wind velocity.

A first type of model was developed in [19] and extended later [20–22]. The dynamics of the rivulets, which is represented

* Corresponding address: GEMICO-ENSIC, Nancy Université, 1 rue Grandville, BP 451, 54001 Nancy Cedex, France.

E-mail address: cecile.lemaitre@ladhyx.polytechnique.fr (C. Lemaitre).

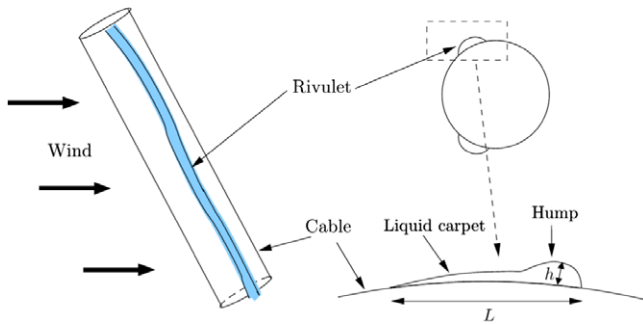


Fig. 1. The presence of two water rivulets along a cable subject to RWIVs. A rivulet is formed of a liquid hump that moves on a liquid carpet during the cable oscillation.

using one or two extra degrees of freedom, renders the cylinder cross-section aerodynamically unstable for certain wind–cable configurations. With these models, the RWIV dependence on the wind speed and cable incline is verified.

Macdonald and Larose [23,24] proposed a new model of dry galloping for inclined cables. The originality of their work is to have taken into account the dependence of the aerodynamic forces on the Reynolds number when the flow is within the critical Reynolds number range, $2.9 \times 10^5 < Re < 3.5 \times 10^5$, for which the drag crisis occurs. Their results show a limited interval of Reynolds number in which the system becomes unstable and the cables happen to vibrate. It has been suggested [16,25,26] that the rivulets add roughness to the cylinder and that the critical Reynolds number range is consequently shifted down to around 1.3×10^5 , which is a Reynolds number typical of RWIVs. Therefore, it is possible that RWIVs could be related to dry inclined galloping. This scenario is in agreement with experimental observations on inclined cables [8, 9], for which vibrations occurred in the wind but were largely amplified in the presence of rivulets.

For both these types of model, the rivulets play a major role. In the former, their dynamics is fully taken into account, and in the latter, they act as amplifiers. But all authors have so far assumed that the rivulets exist. Furthermore, when the rivulets' dynamics was taken into account, their position was also assumed to be known.

1.3. Paper outline

In a previous work [27,28], the authors of the present paper derived a model for the evolution of a liquid film surrounding a cylinder swept by an air flow. The model was used [29] to study the appearance of rivulets for a simplified configuration with a cylinder aligned with the wind direction. The model was able to predict the formation of two rivulets from the film, provided that the wind speed was large enough to overcome the effect of gravity. The position of the rivulets could also be determined. The results were compared successfully to experimental measurements.

This paper is focused on generalising these results to an arbitrary wind–cable configuration and on answering the following questions.

- (i) For a given wind speed, how many rivulets exist? Above which wind speed does the upper rivulet, reputedly responsible for RWIVs, appear?
- (ii) At which positions do the rivulets form?
- (iii) Above which wind speed do the rivulets, and thus the cable oscillations, disappear?

After defining the geometry of the system (Section 1.4), the results obtained in the simplified wind–cable configuration are recalled in Section 2. Arbitrary wind–cable configurations are addressed in Section 3. In Section 3.1, the general expression of the

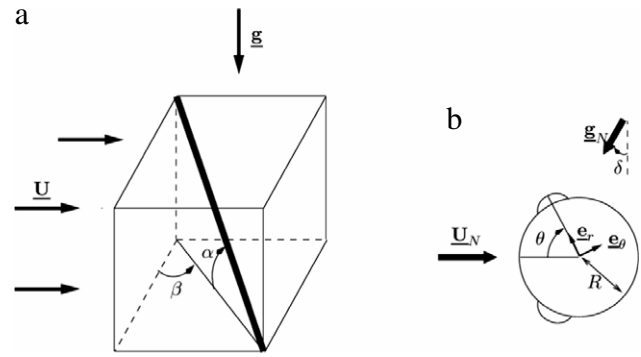


Fig. 2. (a) Geometry of RWIVs. The cables are inclined at an angle α with respect to the horizontal and at β with respect to the wind direction. (b) The projection of the wind speed \underline{U}_N and of the gravity \underline{g}_N in a cable cross-section forms an angle $\delta + \pi/2$.

model is given. The number of rivulets and their position is discussed in Section 3.2. In Section 3.3, a lower limit for the existence of the upper rivulet is predicted and compared to experimental results in the literature. An estimate of the upper limit is proposed in Section 3.4. In Section 3.5, the analytical interval of existence is finally compared to all available experimental data in the literature.

1.4. Problem geometry

We consider a cylinder of radius R , which is inclined at an angle α to a horizontal plane. The air flow speed \underline{U} forms a yaw angle β with the cylinder, as indicated in Fig. 2(a). The projections of the wind speed \underline{U}_N and the gravity vector \underline{g}_N on a plane perpendicular to the cable's axis have a modulus

$$U_N = U \sqrt{\cos^2 \beta + \sin^2 \beta \sin^2 \alpha}, \quad g_N = g \cos \alpha, \quad (1)$$

and form an angle $\delta + \pi/2$, with

$$\delta = \arctan(\sin \alpha \tan \beta). \quad (2)$$

The position on the cylinder is measured in the polar frame $(\underline{e}_r, \underline{e}_\theta)$ in which the origin is taken to be on the cylinder axis. The azimuth θ is measured from the normal wind direction \underline{U}_N/U_N ; see Fig. 2(b).

2. Particular wind–cable configuration

In a previous study, the behaviour of a liquid film flowing around a cylinder immersed in an air flow was investigated by the authors [27–29]. The two-dimensional unsteady Navier–Stokes equations were combined with the lubrication assumptions that the film is thin and that its thickness varies slowly with θ . A particular configuration was considered [29] with $\alpha \neq 0$ and $\beta = \pi/2$, so that $U_N = U \sin \alpha$, $g_N = g \cos \alpha$ and $\delta = \pi/2$. A partial differential equation was obtained, governing the evolution of the film thickness, which reads

$$H, \tau = [H^3 \sin(\theta)],_{,\theta} - Bo^{-1} [H^3 (H, \theta + H, \theta\theta\theta)],_{,\theta} + \frac{1}{2} \mathcal{M} F_{RN}^2 \left[H^3 C_{p, \theta} - H^2 \frac{3}{2\epsilon} C_f \right]_{,\theta}, \quad (3)$$

where $H(\tau, \theta) = h(t, \theta)/h_0$ is the ratio of the film thickness to the initial thickness h_0 and (\cdot) stands for differentiation in time or space. The dimensionless time $\tau = (g_N h_0^2 / 3\nu R) t$ is formed with gravity and the liquid viscosity ν . The first term in the right-hand side represents the effect of gravity on the film; the second term is due to surface tension, and its magnitude is given by the value of the Bond number, $Bo = \rho g_N R^3 / \gamma h_0$ with γ as the air–liquid surface tension and ρ as the liquid density; the effect of wind is contained in the last term, with the density number $\mathcal{M} = \rho_a / \rho$ and

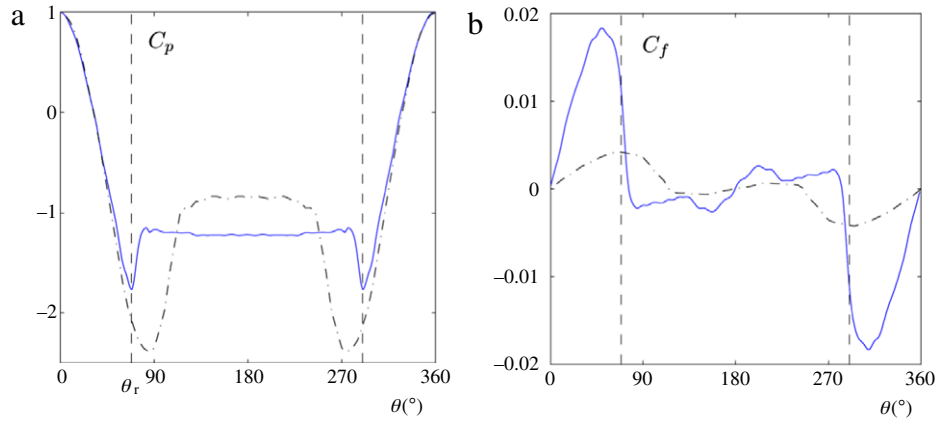


Fig. 3. Aerodynamic coefficients on a smooth and dry cylinder measured by [30] for (—) $Re = 10^5$ and (---) $Re = 3.6 \times 10^6$. (a) Pressure coefficient. (b) Friction coefficient. (---) Position of the center of the rivulets θ_r for $Re = 10^5$.

the Froude number $F_{RN} = U_N / \sqrt{g_N R}$, where ρ_a is the air density. The pressure and friction coefficients are defined with the normal wind speed

$$C_p = \frac{p}{\frac{1}{2} \rho_a U_N^2} \quad \text{and} \quad C_f = \frac{\tau_w}{\frac{1}{2} \rho_a U_N^2}, \quad (4)$$

where p is the pressure and τ_w the tangential constraint at the wall. The small parameter $\varepsilon = h_0/R$ compares the characteristic thickness to the cable's radius.

In the absence of simultaneous pressure and friction measurements on a wet cylinder, the authors used the coefficient distributions measured on a smooth and dry cylinder [30]; see Fig. 3. This approximation is acceptable provided that the rivulet free surface is not too steep. Two representative Reynolds numbers were considered, $Re = 10^5$ and $Re = 3.6 \times 10^6$. For $Re = 10^5$, which is a common value for RWIVs, the flow is sub-critical, meaning that the boundary layer is laminar. At $Re = 3.6 \times 10^6$, the boundary layer is turbulent, and the flow is said to be super-critical. At transition between the sub-critical and super-critical régimes, $2.9 \times 10^5 < Re < 3.5 \times 10^5$, the drag coefficient drops severely. With a protuberance such as a rivulet standing on the cylinder surface, the transition of the boundary layer flow from laminar to turbulent occurs at a lower Reynolds number [31,32], so the flow may be super-critical in RWIV conditions. This is why the C_p and C_f distributions for a super-critical flow, $Re = 3.6 \times 10^6$, on a smooth and dry cylinder were also considered. Within a given régime, sub-critical or super-critical, the C_p and C_f distributions depend weakly on Re .

Eq. (3) has been scaled with gravity, so it is only valid if the projected gravity is not infinitely small, $g_N > 0$. If this holds, the Bond number can be considered to be much lower than the wind coefficient $Bo \ll \mathcal{M}F_{RN}^2$. The thickness growth rate at early times, $r(\theta) = H_{,\tau}(\tau = 0, \theta)$, was obtained by linearising Eq. (3) around the initial profile $H = 1$,

$$r(\theta) = \cos(\theta) + \frac{1}{2} \mathcal{M}F_{RN}^2 \mathcal{F}(\theta). \quad (5)$$

The first term in Eq. (5) is due to gravity and is maximal for $\theta = 0$. The second term is due to wind and is a function of the Froude number. Function \mathcal{F} varies with the azimuth θ through the space derivatives of the pressure and friction coefficients,

$$\mathcal{F}(\theta) = C_{p,\theta\theta} - \frac{3}{2\varepsilon} C_{f,\theta}. \quad (6)$$

This function is maximum at two positions, θ_r and $2\pi - \theta_r$, that are symmetric with respect to the projected wind direction, \mathbf{U}_N/U_N ; see Fig. 4. The locations of the maxima depend on the Reynolds number through C_p and C_f .

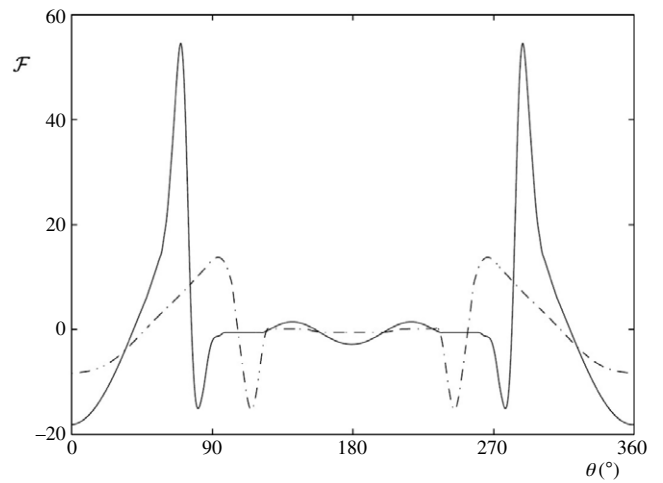


Fig. 4. Shape of the wind function \mathcal{F} versus the azimuth θ , Eq. (6). The maxima of \mathcal{F} determine the rivulets' position at high wind speeds. (—) Sub-critical wind load, $Re = 10^5$, with $\max(\mathcal{F}) = 54.5$ attained at $\theta_r = 71^\circ$ and 289° ; (---) super-critical wind load, $Re = 3.6 \times 10^6$, with $\max(\mathcal{F}) = 13.7$ for $\theta_r = 94^\circ$ and 266° .

For a low wind coefficient $\mathcal{M}F_{RN}^2 \ll 1$, gravity has a dominant effect and the maximum of r is attained at $\theta = 0$. At high Froude numbers $\mathcal{M}F_{RN}^2 \gg 1$, wind dominates and r has two maxima of equal magnitude at θ_r and $2\pi - \theta_r$; see Fig. 5(a).

We then assume that the rivulets form at the locations where the growth rate is maximal. When increasing $\mathcal{M}F_{RN}^2$, the cylinder first exhibits a single gravity-induced rivulet at $\theta = \delta - \pi/2$ and then two wind-induced rivulets at θ_r and $2\pi - \theta_r$. In this cable-wind configuration both rivulets have the same altitude, so there is no upper or lower rivulet.

The transition between the gravity and wind régimes was evaluated by equating the growth rate values at the position of the gravity-induced rivulet $\theta = \delta - \pi/2$ and at the positions of the wind-induced rivulets, θ_r and $2\pi - \theta_r$, yielding a minimal Froude number for the existence of two simultaneous wind-controlled rivulets

$$\mathcal{M}F_{RN,\min}^2 = \frac{2[1 - \cos(\theta_r)]}{C_{p,\theta\theta}(\theta_r) - \frac{3}{2\varepsilon} C_{f,\theta}(\theta_r)}. \quad (7)$$

This minimal Froude number is compared to experimental measurements in Fig. 5(b). The predicted transition is shown to give a very realistic lower bound for the appearance of two rivulets due to wind. After the transition, the rivulets shift leeward until they reach an asymptotical position which is very well predicted by the model.

Table 1
Parameter values for experiments in the literature.

Authors	R (m)	α (°)	β (°)	$\mathcal{M}F_{RN,min}^2$	Bo^{-1}
Seidel (2004) [21]	5.5×10^{-2}	80	90	4.7×10^{-2}	1.3×10^{-4}
Matsumoto (1992) [34]	7.5×10^{-2}	40	45	9.5×10^{-2}	1.2×10^{-5}
Hikami (1980) [7]	7×10^{-2}	45	45	1.6×10^{-1}	1.5×10^{-5}
Wang (2005), $Q = 8$ L/h [33]	2.25×10^{-2}	45	0	2.6×10^{-1}	4.6×10^{-4}
Wang (2005), $Q = 8$ L/h [33]	2.25×10^{-2}	45	45	3.9×10^{-1}	4.6×10^{-4}
Wang (2005), $Q = 1.4$ L/h [33]	2.25×10^{-2}	45	45	4.5×10^{-1}	4.6×10^{-4}
Gu (2005) [14]	6×10^{-2}	25–45	25–45	6.9×10^{-2}	1.9×10^{-5}

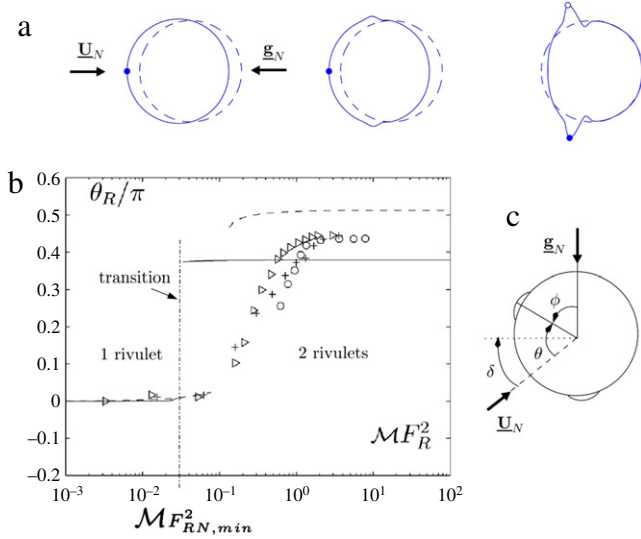


Fig. 5. (a) Growth rate in polar coordinates with arbitrary scale; from left to right, $\mathcal{M}F_{RN}^2 = 0, 10^{-2}$ and 10 . (b) Position of one rivulet as a function of $\mathcal{M}F_{RN}^2$; a symmetrical rivulet exists at $-\theta_r$; Eq. (7) with (–) a sub-critical wind load, $Re = 10^5$, and (–) a super-critical wind load, $Re = 3.6 \times 10^6$; (▷), (+) and (◊) experiments [29]; (– · –) transition given by Eq. (7) for $Re = 10^5$. (c) Definition of angle ϕ with respect to the gravity direction.

3. General wind–cable configuration

3.1. Lubrication model

In the general configuration with arbitrary wind and gravity orientations, the partial differential equation describing the evolution of the film thickness reads

$$H_{,\tau} = [H^3 \cos(\theta - \delta)]_{,\theta} - Bo^{-1} [H^3 (H_{,\theta} + H_{,\theta\theta\theta})]_{,\theta} + \frac{1}{2} \mathcal{M}F_{RN}^2 \left[H^3 C_{p,\theta} - H^2 \frac{3}{2\epsilon} C_f \right]_{,\theta}. \quad (8)$$

In the case of a stay cable in RWIV conditions, the inverse of the Bond number is very small, $Bo^{-1} \ll 1$ and $Bo^{-1} \ll \mathcal{M}F_{RN}^2$, as shown in Table 1. The term due to surface tension is subsequently neglected and only gravity and wind actions are retained. Eq. (8) is then linearised at early times to yield the thickness growth rate for an arbitrary angle δ :

$$r(\theta) = -\sin(\theta - \delta) + \frac{1}{2} \mathcal{M}F_{RN}^2 \mathcal{F}(\theta). \quad (9)$$

The gravity term is a function of δ and is maximum for $\theta = \delta - \pi/2$. As the problem is described in the wind-oriented reference frame ($\mathbf{e}_r, \mathbf{e}_\theta$), the wind term is independent of δ and the shape of \mathcal{F} is unchanged; see Fig. 4.

3.2. Rivulets' number and position

At low Froude numbers, that is, in the dominant gravity régime $\mathcal{M}F_{RN}^2 \ll 1$, the growth rate is maximal at $\theta = \delta - \pi/2$, and only

one rivulet exists at this position. In the wind-controlled régime, $\mathcal{M}F_{RN}^2 \gg 1$, the growth rate has two maxima of nearly equal magnitude at θ_r and $2\pi - \theta_r$, corresponding to two rivulets. In the particular cases $\delta = \pm\pi/2$, both rivulets have the same altitude. For other values of δ , one of the rivulets, located at θ_{up} , has a higher altitude than the other, and will be referred to as the upper rivulet. Experimental work reported in the literature has shown that it is the upper rivulet which is responsible for RWIVs [7]. This work therefore focuses on the upper rivulet. The upper rivulet can be identified by a negative scalar product of the unit radius vector with the projected gravity $\mathbf{e}_r(\theta_{up}) \cdot \mathbf{g}_N = g_N \sin(\theta_{up} - \delta) < 0$. Its position is $\theta_{up} = \theta_r$ if $-\pi/2 < \delta < \pi/2$ and $\theta_{up} = 2\pi - \theta_r$ if $\pi/2 < \delta < 3\pi/2$. The growth rate r reaches its secondary minimum at θ_{up} . The lower rivulet, identified with $\mathbf{e}_r(\theta_{low}) \cdot \mathbf{g}_N = g_N \sin(\theta_{low} - \delta) > 0$, appears at the location $\theta_{low} = 2\pi - \theta_r$ if $-\pi/2 < \delta < \pi/2$ and $\theta_{low} = \theta_r$ if $\pi/2 < \delta < 3\pi/2$ and corresponds to the global maximum of r .

The initial film thickness has been set to $h_0 = 5 \times 10^{-4}$ m and the cylinder radius to $R = 0.1$ m, so $\epsilon = 5 \times 10^{-3}$. For a sub-critical flow ($Re = 10^5$), the rivulets are expected to grow at $\theta_r = 71^\circ$ and 289° . For a super-critical flow ($Re = 3.6 \times 10^6$), the locations predicted by the model move downstream to $\theta_r = 94^\circ$ and 266° . For a given régime, sub-critical or super-critical, the predicted positions vary little with the wind speed due to the weak dependence of C_p and C_f on Re .

These positions, obtained from the linear analysis of Sections 2 and 3.1, can be compared to the positions predicted by the nonlinear numerical approach of [28]. In the latter case, for high wind speeds, the rivulets appear at $\theta_r = 68^\circ$ and 292° for a sub-critical wind load and at $\theta_r = 91^\circ$ and 269° for a super-critical wind load, which are very close to the linear values. This good agreement shows the relevance of the linear approach.

In the literature, the 0° reference for the angular position of the rivulets differs among the authors. Here, we express the rivulets' position with respect to the direction of the projected gravity \mathbf{g}_N/g_N with an angle ϕ that is connected to δ and θ by

$$\phi = \delta + \pi/2 - \theta, \quad (10)$$

as shown in Fig. 5(c). In Fig. 6, the theoretical and experimental values of ϕ are compared at high wind speeds as a function of δ . The experiments were performed with varying yaw angle, different cable incline and at several water rates (i.e. several rivulet dimensions) [7, 14, 21, 29, 33, 34]. For tests conducted with different wind speeds, only the points at the highest wind speeds are shown because they correspond to the wind-controlled régime. The predictions are in good agreement with the experiments.

3.3. Lower limit for the existence of wind-controlled rivulets

At the transition between the gravity and wind régimes, the growth rate value at the position of the gravity-induced rivulet $\theta = \delta - \pi/2$ and its value at the position of the upper wind-induced rivulet, θ_r or $2\pi - \theta_r$, are taken to be equal, as in the simplified configuration; see Fig. 7. The minimal Froude number for the existence of two wind-controlled rivulets and thus of an

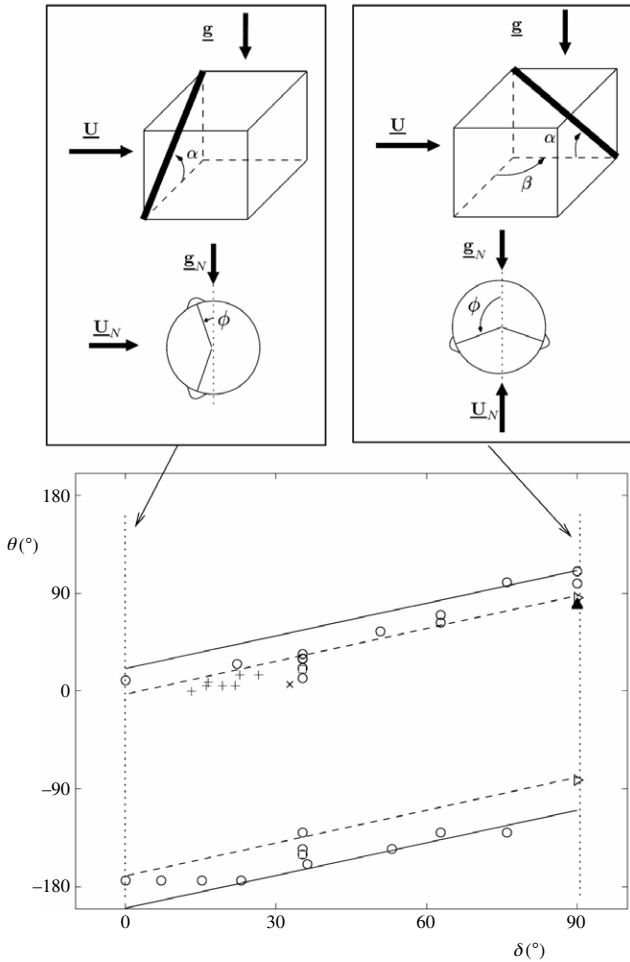


Fig. 6. Position of the rivulets defined from the projected vertical. Theoretical values obtained for (–) a sub-critical wind load $Re = 10^5$ and (– –) a super-critical wind load, $Re = 3.6 \times 10^6$. Measurements at high wind speeds from (□) [7], (×) [34], (▷) [21], (○) [33], (+) [14] and (▲) [29].

upper rivulet ($\delta \neq \pm\pi/2$) is thus

$$\mathcal{M}F_{RN,\min}^2 = \frac{2 [1 + \sin(\theta_{up} - \delta)]}{C_{p,\theta\theta}(\theta_{up}) - \frac{3}{2\epsilon} C_{f,\theta}(\theta_{up})}. \quad (11)$$

This limit is a function of angle δ .

An inferior bound for the existence of two simultaneous rivulets, including the upper rivulet, may also be defined more qualitatively by considering the Froude number at which the maxima of the gravity and the wind terms, considered independently in Eq. (9), are equal:

$$\max(-\sin(\theta - \delta)) = \max\left(\frac{1}{2} \mathcal{M}F_{RN}^2 \mathcal{F}(\theta)\right). \quad (12)$$

This leads to a critical number independent of δ :

$$(\mathcal{M}F_{RN,\min}^2)' = \frac{2}{\max[\mathcal{F}(\theta)]}. \quad (13)$$

If an initial film thickness $h_0 = 5 \times 10^{-4}$ m is assumed, and a cable radius $R = 0.1$ m, the maximum of the function \mathcal{F} is found to be 54.5 for $Re = 10^5$ with comparable contributions of pressure, $\partial_\theta^2 C_p = 25.5$, and friction, $-\frac{3}{2\epsilon} \partial_\theta C_f = 29.0$, corresponding to a minimal Froude number $\mathcal{M}F_{RN,\min}^2 = 4.3 \times 10^{-2}$ for $\delta = 60^\circ$ or $(\mathcal{M}F_{RN,\min}^2)' = 3.7 \times 10^{-2}$. For a super-critical régime, $Re = 3.6 \times 10^6$, the wind function reaches the maximum value

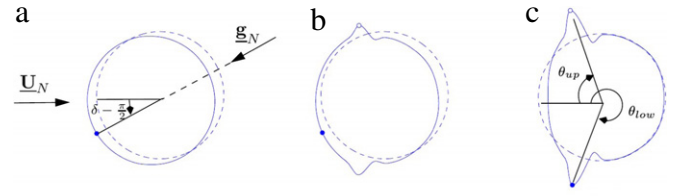


Fig. 7. Thickness growth rate in the polar frame oriented in the wind direction for $\delta - \pi/3$. (–) Growth rate with arbitrary scale (a) for a dominant gravity, $\mathcal{M}F_{RN}^2 = 0$; (b) at the transition between gravity and wind régimes, $\mathcal{M}F_{RN,\min}^2 = 4.3 \times 10^{-2}$, Eq. (11); (c) for a dominant wind load, $\mathcal{M}F_{RN}^2 = 10$.

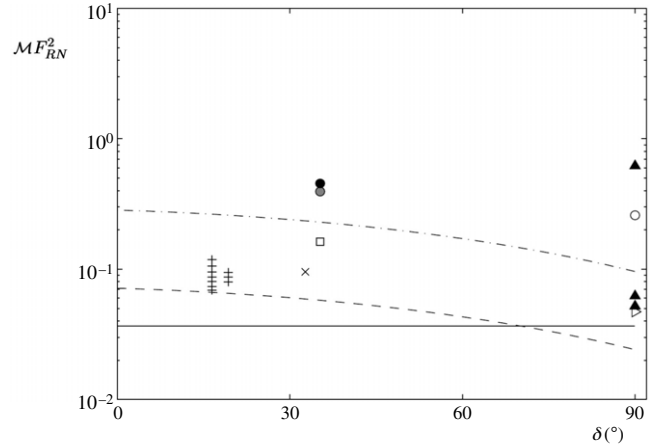


Fig. 8. Lower limit for the existence of wind-generated rivulets. Normal Froude number $\mathcal{M}F_{RN}^2$ as a function of the gravity–wind orientation δ . Theoretical minimum value from Eq. (11) for (–) $Re = 10^5$ and (– · –) $Re = 3.6 \times 10^6$. (–) Qualitative limit $(\mathcal{M}F_{RN,\min}^2)' = 3.6 \times 10^{-2}$ given by Eq. (13) for $Re = 10^5$. Measurements with different cable radius and orientation: (□) $\beta = 45^\circ$, $Re = 87\,300$ [7]; (×) $\beta = 45^\circ$, $Re = 79\,600$ [34]; (▷) $\beta = 90^\circ$, $Re = 15\,000$ [21]; (○) $\beta = 0^\circ$, $Re = 24\,600$, water rate feeding the rivulets $Q = 8.0$ L/h, ● $\beta = 45^\circ$, $Re = 24\,500$, $Q = 8.0$ L/h and (●) $\beta = 45^\circ$, $Re = 26\,600$, $Q = 1.4$ L/h [33]; (+) $\beta = 25^\circ$ – 45° and $Re = 56\,000$ [14]; (▲) $\beta = 90^\circ$ and $Re = 1500$ – 2900 [29].

$\max(\mathcal{F}) = 13.7$, with $\partial_\theta^2 C_p = 11.6$ and $-\frac{3}{2\epsilon} \partial_\theta C_f = 2.1$, leading to $\mathcal{M}F_{RN,\min}^2 = 1.7 \times 10^{-1}$ for $\delta = 60^\circ$ and $(\mathcal{M}F_{RN,\min}^2)' = 1.5 \times 10^{-1}$.

In Fig. 8, limits (11) and (13) for the rivulets' existence are compared to all experimental data available in the literature. The Froude number is represented as a function of δ . For the tests performed at different wind speeds, the points corresponding to the lowest speed for which two simultaneous rivulets were observed are retained. Both minimum theoretical Froude numbers obtained for sub-critical conditions are found to be lower than all the experimental values and thus provide very realistic inferior boundaries for the existence of two water rivulets on a cable subject to wind. The use of a super-critical wind load, however, leads to an overestimation of the limit. In the rest of the paper, Eq. (13) will be used with a sub-critical wind load as the theoretical lower limit for the existence of the upper rivulet.

The lower limit can also be expressed in terms of the normal Weber number, $We_N = \rho_a U_N^2 R / \gamma$, where γ is the surface tension. The Froude and the Weber numbers are linked by

$$We_N = \mathcal{M}F_{RN}^2 \left(\frac{R}{\ell_c}\right)^2 \cos \alpha, \quad (14)$$

where $\ell_c = \sqrt{\gamma / (\rho g)}$ is the capillary length, comparing the surface tension to gravity. The minimum Weber number for the appearance of the rivulets is obtained from Eq. (13)

$$We_{N,\min} = \frac{2 \cos \alpha}{\max(\mathcal{F})} \left(\frac{R}{\ell_c}\right)^2. \quad (15)$$

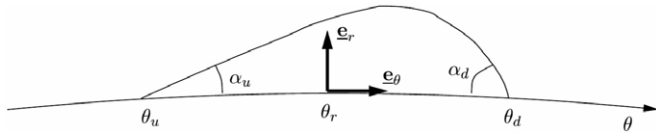


Fig. 9. Rivulet on a cylinder subject to wind action. The rivulet has an upstream contact angle α_u and a downstream contact angle α_d .

3.4. Upper limit for the existence of rivulets

3.4.1. Force balance on a rivulet

In the laboratory [15,33], it has been observed that the rivulets do not exist at high wind speeds. Indeed, if U is raised above a critical value U_{max} , liquid detaches from the rivulets and they vanish. Until this happens, each rivulet is held on the cylinder's wall due to surface tension at the air–water–solid contact lines that produces a global force \mathbf{F}_{st} on the rivulet. The drag force \mathbf{D} that tends to pull a rivulet away is azimuthal and is mainly due to friction. The rivulets remain at equilibrium until break-off occurs, so the projection on \mathbf{e}_θ of the sum of the two forces is close to zero:

$$(\mathbf{D} + \mathbf{F}_{st}) \cdot \mathbf{e}_\theta \approx 0. \tag{16}$$

To estimate the value of U_{max} , we assume the occurrence of break-off will start when the triple line can no longer remain static.

3.4.2. Contact forces

We consider the section of a rivulet flowing along a cylinder; see Fig. 2. The upstream and downstream contact angles are α_u and α_d , respectively; see Fig. 9. At the triple lines, contact forces are active along the tangent line with a magnitude γ for a unit length of rivulet [35]. When projected on \mathbf{e}_θ , this leads to

$$\mathbf{F}_{st} \cdot \mathbf{e}_\theta = \gamma (\cos \alpha_d - \cos \alpha_u) \tag{17}$$

where γ is the air–water surface tension coefficient. We assume that, at the very limit of break-off, the contact angles reach the receding, α_r , and the advancing, α_a , hysteresis values,

$$\alpha_u = \alpha_r, \quad \alpha_d = \alpha_a. \tag{18}$$

The receding and advancing contact angles depend on the nature of the gas, liquid and solid that are used. They are also very sensitive to the state of the solid surface. To measure these angles in the case of water standing on a cable in air, the following experiment was set up. A real stay cable polyethylene casing was obtained from the company Bouygues Travaux Publics, and the shield was left outdoors for a few months so that it was dirtied by pollution and acquired realistic wetting characteristics. A water drop is formed on the casing. A micrometric syringe pump is used to fill up (resp. empty) the drop in a slow quasi-static manner, Fig. 10. While the drop volume increases (resp. decreases), the

contact angles grow (resp. decrease) but the contact line remains static. This is pursued until a maximum (resp. minimum) angle is reached, the advancing angle (resp. receding angle) and the contact line suddenly moves and the drop expands (resp. retracts). The new contact angle is below (resp. above) the advancing (resp. receding) angle. The drop is filmed from the side with a camera and the angles are measured with a simple geometrical method just before the triple lines begins to move.

The advancing and receding angle values are found to be

$$\alpha_a = 87 \pm 2^\circ, \quad \alpha_r = 25 \pm 2^\circ. \tag{19}$$

3.4.3. Drag force

The drag per unit length that acts on a rivulet is sought under the shape

$$D = \frac{1}{2} \rho_a U^2 \mathcal{L}_D. \tag{20}$$

Factor \mathcal{L}_D has the dimension of a length and its value is discussed in this section.

We consider a rivulet centered on one of the maxima, θ_r , of function \mathcal{F} . At the rivulet's angular position, the pressure coefficient C_p reaches its minimum value and is symmetric with respect to the rivulet's centerline in a first approximation; see Fig. 3(a). Because of this symmetry, the contribution of C_p to the azimuthal force acting on the rivulet is almost zero. The drag that acts on the rivulet is mainly due to friction, so the drag length reads

$$\mathcal{L}_D = \left\| \int_{\theta_u}^{\theta_d} C_f(\theta) R d\theta \mathbf{e}_\theta \right\| \approx L \overline{C}_f, \tag{21}$$

where θ_u and θ_d are the azimuth of the upstream and downstream contact lines, respectively. The rivulet's width $L = R(\theta_d - \theta_u)$ and the average friction coefficient

$$\overline{C}_f = \frac{1}{\theta_d - \theta_u} \int_{\theta_u}^{\theta_d} C_f(\theta) d\theta \tag{22}$$

have been introduced.

Another way to estimate \mathcal{L}_D is to consider the aerodynamic drag that acts on an imperfection standing on a surface. In particular, a joint holding two metal sheets together has a shape close to that of a rivulet and its drag has been measured on a flat plate [36,32]. In these experiments, the plate was swept by an air flow and the joint was located at a distance x from the leading edge. The boundary layer was assumed to be turbulent and the joint height to be lower than the boundary thickness. In the present case, the rivulets are located on a cylinder that, as such, exhibits no leading edge. Nevertheless, we replace x by the circular distance

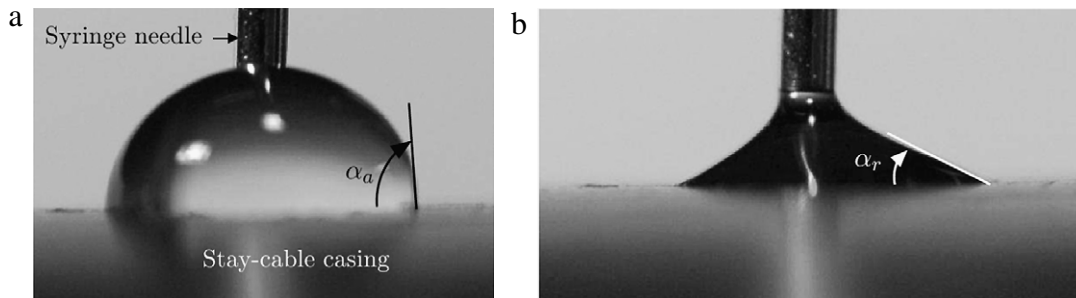


Fig. 10. Measurement of the advancing and receding angles of a water drop standing on a cable casing made of polyethylene. The drop volume is increased slowly with a syringe; the contact angles grow until they reach the advancing angle for which the triple line slips and the drop spreads out. (a) Drop in which triple line is about to advance; (b) drop in which triple line is about to retract.

between a rivulet (located at θ_r) and the stagnation point (at $\theta = 0$), $x \approx \theta_r R$. By analogy, the drag length is estimated to be

$$\mathcal{L}_D = \eta h \left(\frac{h}{x} \right)^{1/3} C_{Do}, \quad (23)$$

where η is a constant and C_{Do} is a specific drag coefficient which value depends on the shape of the protuberance.

The rivulet has a typical width of $L \approx 3$ cm and its height has been chosen to be $h = 1$ mm [17,18]. The stay cable is again assumed to have radius of $R = 0.1$ m. With these dimensions and for $Re = 10^5$, the average friction coefficient, $\overline{C_f}$, Eq. (21), is estimated with the data from [30], $\overline{C_f} \approx 8 \times 10^{-3}$; see Fig. 3(b). The coefficient of Eq. (23) has a value $\eta = 2.97$ and the specific drag coefficient is equal to $C_{Do} = 0.51$ for the joint. As a consequence, the drag length value is $\mathcal{L}_D = 2.4 \times 10^{-4}$ and 3.1×10^{-4} m from Eqs. (21) and (23), respectively. Both estimates of the aerodynamic azimuthal force on a rivulet are thus in agreement.

3.4.4. Maximum wind speed of existence

Using Eqs. (16), (17) and (20), we get an upper limit for the existence of rivulets on a cylinder in the presence of wind:

$$U_{N,\max} = \sqrt{\frac{\gamma (\cos \alpha_r - \cos \alpha_a)}{\frac{1}{2} \rho_a \mathcal{L}_D}}. \quad (24)$$

If expression (21) is retained to compute the drag, the maximum wind speed is proportional to $L^{-1/2}$. On the other hand, if we consider Eq. (23), $U_{N,\max}$ is proportional to $h^{-2/3}$. This indicates that the larger the rivulet, in width L or height h , the lower $U_{N,\max}$. It moreover depends on the nature of the casing through the contact angles. This is consistent with past experiments [15], which showed that for certain cable–wind configurations two rivulets could exist if the surface of the cable was polluted by soot, whereas they could not on a clean surface.

The numerical value of the maximum wind speed is $U_{N,\max} \approx 20.8$ m/s if the drag is computed from Eq. (21) and $U_{N,\max} \approx 18.5$ m/s if computed with Eq. (23). These values should be superior to the maximum wind speed for RWIVs since rivulets are always present during such vibrations. This is the case, as RWIVs are not observed above $U = 17$ m/s [7].

With regards to the result of this section, a new counter-measure for RWIVs is suggested, which is to adjust the wetting properties of the cable casing so as to decrease $U_{N,\max}$ and consequently reduce the wind speed range for which rivulets can exist.

3.5. Comparison with experiments

The upper limit for existence results in the competition between the wind effect, friction, and capillary force. To describe the break-off phenomenon, the appropriate non-dimensional number is the Weber number. The critical normal Weber number for break-off is

$$We_{N,\max} = 2 (\cos \alpha_r - \cos \alpha_a) \frac{R}{\mathcal{L}_D}. \quad (25)$$

Fig. 11 compares the lower and upper limits predicted by Eqs. (15) and (25) with experimental results from the literature as a function of the cable incline. Only the experiments with comparable cable radii $R \approx 6.5$ cm [7,34,21,14] are shown. For tests performed with varying wind speed, only the minimum and maximum speeds for which two rivulets have been observed are reported.

All the experimental values fall into the interval predicted by the models. Both Eq. (15), derived from the lubrication model, and Eq. (25), obtained by equating the contact forces with the drag on the rivulets, give a very good prediction for the existence of two wind-induced rivulets on a wet cable subject to wind, and in particular the upper rivulet that is said to be responsible for RWIVs.

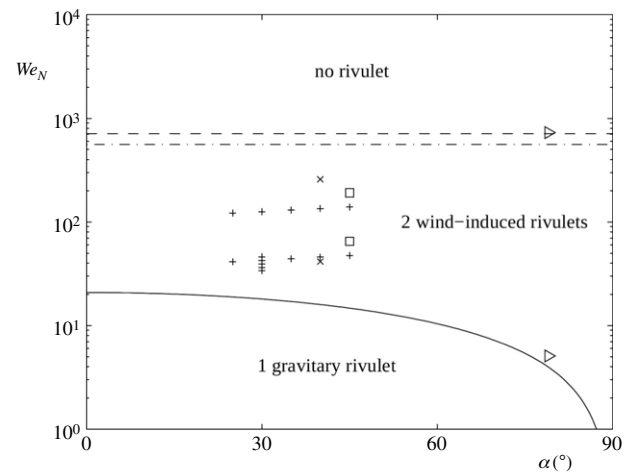


Fig. 11. Interval of existence of the rivulets. Normal Weber number We_N as a function of the cable incline α for a Reynolds number $Re = 10^5$. (—) Lower limit of rivulets' existence from Eq. (15); (---) upper limit of existence from Eqs. (21) and (25); (- · -) upper limit from Eqs. (23) and (25). Extremal measurements of (□) [7], (×) [34], (▷) [21] and (+) [14].

4. Conclusion

The problem of the existence of rivulets on a wet stay cable subject to wind has been addressed. In a former study, a lubrication model was derived. A minimum wind speed for the appearance of two wind-induced rivulets was predicted in a particular wind–cable configuration. In the present paper, all the possible three-dimensional configurations have been considered. The number of rivulets has been shown to depend on the relative magnitude of wind and gravity. At low Froude number, that is, for dominant gravity, only one rivulet exists. At high Froude number, that is for dominant wind, two rivulets exist. One of them is generally located higher than the other: this is the upper rivulet that is claimed to be responsible for RWIVs. The rivulet position predicted by the model was compared successfully with results of former experiments. The transition from the gravity to the wind régime yields a lower limit for the existence of wind-induced rivulets. An upper limit for the existence of the rivulets has been estimated by balancing the friction forces with surface tension forces at the rivulets' triple lines. An interval of existence has thus been proposed and is in good agreement with all the past experimental observations.

Acknowledgements

We would like to thank most warmly Jean-Marc Chomaz for the numerous fruitful discussions and scientific advice. We are indebted to Cédric Ody, who provided some help for the experiment presented in this paper. Finally, we would like to thank the company Bouygues Travaux Publics for their interest and their financial support of this work.

References

- [1] R. Blevins, Flow-Induced Vibration, Van Nostrand Reinhold, New York, 1977.
- [2] E. Naudascher, D. Rockwell, Flow-Induced Vibrations, A.A. Balkema, Rotterdam, 1994.
- [3] E. Simiu, R. Scanlan, Wind Effect on Structures, John Wiley & Sons, Inc., 1996.
- [4] E. de Langre, Fluides et solides, Éditions de l'École Polytechnique, 2001 (in French).
- [5] P. Hémon, Vibrations Couplées avec le Vent, Éditions de l'École Polytechnique, 2006 (in French).
- [6] J. Wiannecki, Cables wind excited vibrations of cable-stayed bridges, in: Pergamon Press, Oxford-New York (Ed.), Proceedings of the 5th International Conference of Wind Engineering, Colorado, 1979, pp. 1381–1393.
- [7] Y. Hikami, N. Shiraishi, Rain-wind induced vibrations of cables in cable-stayed bridges, J. Wind Eng. Ind. Aerodyn. 29 (1988) 409–418.

- [8] M. Matsumoto, N. Shiraishi, M. Kitazawa, C. Knisely, H. Shirato, Y. Kim, M. Sujii, Aerodynamic behaviour of inclined circular cylinders cable aerodynamics, *J. Wind Eng. Ind. Aerodyn.* 33 (1990) 63–72.
- [9] J. Main, N. Jones, Full-scale measurement of stay cable vibration, in: 10th International Conference on Wind Engineering, Copenhagen, Denmark, 1999, pp. 963–970.
- [10] J. Den Hartog, *Mechanical Vibrations*, Dover Publications, Inc., New York, 1985.
- [11] D. Schwarzkopf, G. Sedlacek, Characterization of the main parameters of rain-wind-induced vibrations, in: 11th International Conference on Wind Engineering, Lubbock, Texas, 2003.
- [12] A. Bosdogianni, D. Olivari, Wind- and rain-induced oscillations of cables of stayed bridges, *J. Wind Eng. Ind. Aerodyn.* 64 (1996) 171–185.
- [13] C. Verwiebe, H. Ruscheweyh, Recent research results concerning the exciting mechanisms of rain-wind-induced vibrations, *J. Wind Eng. Ind. Aerodyn.* 74–76 (1998) 1005–1013.
- [14] M. Gu, X. Du, Experimental investigation of rain-wind-induced vibration of cables in cable-stayed bridges and its mitigation, *J. Wind Eng. Ind. Aerodyn.* 93 (1) (2005) 79–95.
- [15] O. Flamand, Rain-wind induced vibration of cables, *J. Wind Eng. Ind. Aerodyn.* 57 (1995) 353–362.
- [16] N. Cosentino, O. Flamand, C. Ceccoli, Rain-wind induced vibration of inclined stay cables. part I: experimental investigation and physical explanation, *Wind Struct.* (2003) 471–484.
- [17] N. Cosentino, Rain-wind induced vibrations of stay cables, Ph.D. Thesis, Bologna, 2002.
- [18] D. Schwarzkopf, Regen-wind-induzierte Schwingungen, Ph.D. Thesis, Institut für Stahlbau, RWTH Aachen, 2004.
- [19] H. Yamaguchi, Analytical study on growth mechanism of rain vibration of cables, *J. Wind Eng. Ind. Aerodyn.* 33 (1990) 73–80.
- [20] N. Cosentino, O. Flamand, C. Ceccoli, Rain-wind induced vibration of inclined stay cables. part II: mechanical modeling and parameter characterisation, *Wind Struct.* (2003) 485–498.
- [21] C. Seidel, D. Dinkler, Mode switching of rain-wind-induced vibrations, in: 21st International Congress of Theoretical and Applied Mechanics, Warsaw, Poland, no. SM25L-12785, 2004.
- [22] U. Peil, N. Nahrath, Modeling of rain-wind induced vibrations, *Wind Struct.* 6 (1) (2003) 41–52.
- [23] J. Macdonald, G. Larose, Two-degree-of-freedom inclined cable galloping—part 1: General formulation and solution for perfectly tuned system, *J. Wind Eng. Ind. Aerodyn.* 96 (2008) 291–307.
- [24] J. Macdonald, G. Larose, Two-degree-of-freedom inclined cable galloping—part 2: Analysis and prevention for arbitrary frequency ratio, *J. Wind Eng. Ind. Aerodyn.* 96 (2008) 308–326.
- [25] G. Larose, S. Zan, The aerodynamic forces on stay cables of cable-stayed bridges in the critical Reynolds number range, in: Fourth International Symposium on Cable Dynamics, Montreal, Canada, 2001, pp. 77–84.
- [26] O. Flamand, J. Peube, P. Papanikolas, An explanation of the rain-wind induced vibration of inclined stays, in: Fourth International Symposium of Cable Dynamics, 2001.
- [27] C. Lemaître, Dynamique d'un film d'eau de pluie sur un hauban de pont soumis au vent, Ph.D. Thesis, École Polytechnique, 2006 (in French).
- [28] C. Lemaître, P. Hémon, E. de Langre, Thin water film around a cable subject to wind, *J. Wind Eng. Ind. Aerodyn.* 95 (9–11) (2007) 1259–1271.
- [29] C. Lemaître, M. Alam, P. Hémon, E. de Langre, Y. Zhou, Rainwater rivulets on a cable subject to wind, *C. R. Méc.* 334 (2006) 158–163.
- [30] E. Achenbach, Distribution of local pressure and skin friction around a circular cylinder in a cross-flow up to $Re = 5 \times 10^6$, *J. Fluid Mech.* 34 (4) (1968) 625–639.
- [31] E. Szechenyi, Supercritical Reynolds number simulation for two-dimensional flow over circular cylinders, *J. Fluid Mech.* 70 (3) (1975) 529–542.
- [32] S. Hoerner, *Fluid Dynamic Drag*, Bricktown, 1965.
- [33] Z. Wang, Y. Zhou, J. Huang, Y. Xu, Fluid dynamics around an inclined cylinder with running water rivulets, *J. Fluids Struct.* 21 (1) (2005) 49–64.
- [34] M. Matsumoto, N. Shiraishi, H. Shirato, Rain-wind induced vibration of cables of cable-stayed bridges, *J. Wind Eng. Ind. Aerodyn.* 43 (1992) 2011.
- [35] G. De Gennes, F. Brochard-Wyart, D. Quéré, *Capillarity and Wetting Phenomena: Drops, Bubbles, Pearls, Waves*, Springer, New York, 2004.
- [36] K. Wieghardt, Erhöhung des turbulenten Reibungswiderstandes durch Oberflächenstörungen, *Tech. Rep.* 1563, ZWB, deutschen Luftfahrtforschung, 1943.